Numerical Analysis of the Shock Train Evolution in Planar Nozzles with Throat Length

San Luis Tolentino

Research collaborator
Group of Mathematical Modeling and
Numerical Simulation (GMMNS)
National University of Engineering (UNI)
Lima
Perú

Jorge Mírez

Elec. Mech, Eng.; MSc & Dr Physics
Professor
Group of Mathematical Modeling and
Numerical Simulation (GMMNS)
National University of Engineering (UNI)
Lima
Perú

Simón A. Caraballo

Professor
UNEXPO Polytechnic University
Department of Mechanical Engineering
Bolívar
Venezuela

In the present investigation, the behavior of compressible flow in planar nozzles with throat length is analyzed to determine the flow velocity range and pressure fluctuations in the throat section. The flow field was simulated in 2D computational domains with the ANSYS-Fluent R16.2 code. The RANS model was applied for steady-state flow. The governing equations used are the conservation of mass, momentum, energy, and the ideal gas equation of state. The Sutherland equation was used for the viscosity as a function of temperature. The Spalart-Allmaras turbulence model was used to model the flow turbulence, which was validated with experimental pressure data. In the throat section, for the central region of the flow, as the throat length increases, the flow fluctuates and decelerates. Oblique shock waves are produced, and a shock train region is formed. The flow velocity is transonic and is in the Mach number range of 1 to 1.2, and the static pressure is in the range of 0.37 to 0.52. Therefore, as a result of flow fluctuations, throat length has a significant effect on flow development.

Keywords: Flow fluctuations, Oblique shock waves, Planar nozzle, Simulation, Shock train, Throat length, Transonic flow.

1. INTRODUCTION

The study of compressible and viscous flow behavior for different geometries of supersonic nozzles applied to the aerospace area is recurrent [1-3]. The most prominent convergent-divergent supersonic nozzles are bell nozzles [1,3-5], conical nozzles [1,5-9] and planar nozzles [10-13]. For conical nozzles, the optimal range of the half angle, α, is between 12° and 18°. For α < 12°, the nozzles are considered off-design [1,9], and the same principle applies to planar nozzles.

Research in the study of compressible flow encom–passes geometrical concepts of the throat section and the contours of converging and diverging walls [1,9,14-16]. Also, compressible flow research extends to obtaining mathematical models of approximate solutions for analytical equations that are implicit and impossible to invert by algebraic procedures [17-20].

The flow behavior is studied at different nozzle pressure ratios (NPR), where the flow pressure condi–tions at the nozzle inlet and outlet condition the flow to be overexpanded, adapted, or under-expanded [1]. The nozzles are designed for an adapted flow [1,16], and there are no shock waves at the divergent and exit of the nozzle. When the NPR is larger than the adapted flow, then you have an under-expanded flow. When there are shock waves at the divergent of the nozzle, the flow is said to be overexpanded, the NPR being much smaller with respect to the adapted flow [1,16].

In an overexpanded flow, shock wave structures

such as oblique shocks, reflected shocks, internal shocks, and the normal shock front are affected by the curvature of the diverging nozzle wall. In the central region of the flow, at the normal shock wave front, sharp jumps in velocity decrease, and increases in tem–perature and pressure occur after flow braking [21].

After the shock, for the flow region adjacent to the wall, flow separation, flow recirculation, and adverse pressure gradients occur; therefore, the velocity and temperature gradients of the boundary layer are affected [21]. The turbulent boundary layer interacts with the shock wave, which causes instability in its position. In addition, it is present in the flow turbulence, rough wall effect, wall temperature effect, vortices, free shock separation (FSS), and restricted shock separation (RSS), as well as the distri–bution of lateral pressure loads on the nozzle walls [21-24]. In the flow zones adjacent to the profiled walls, Prandlt-Meyer expansion waves occur [21]. Using the Schlieren technique [25], images of the shock waves are captured. Using computational fluid dynamics (CFD) [26], the tur–bulence of the flow field is simulated to obtain approxi–mate solutions. Studies of compressible flow behavior in off-design planar nozzles have reported different configu–rations of the shock wave structure. Flow studies for planar nozzles with symmetric geometry for the experimental case were reported by Hunter [10] and Zebiri et al. [27] for the case of numerical simulations by Tolentino [28] and Tolentino et al. [29]. Experimental studies of the flow in planar nozzles with asymmetric geometry have been reported by Verma and Manisankar [30] and for doubly divergent nozzles by Arora and Vaidyanathan [11].

As the half angle α decreases, the shock wave pro–pagation forms a set of oblique and reflected waves called shock train [34], which is the result of the interaction of the turbulent boundary layer with the shock wave (SWTBLI) due to pressure variations. At the beginning of

the propagation, the fluctuation intensity is higher, and at the end, the intensity is lower. Such flow development has been reported by Kameli et al. [31], Giglmaier et al. [32], and Vignesh et al. [35]. Also, Matsuo et al. [34], Wang et al. [35], and Xue et al. [36] have carried out studies on the compressible flow in parallel-walled ducts and reported the presence of the shock train.

Conical nozzles with straight-cut throats have appli–cations in high-power solid-fuel rocket engines as well as in experimental engines of the amateur category [37]. Where the length L_m of the solid fuel rocket engine comprises the combustion chamber, which is a cylinder of given length, and the nozzle which is coupled to the combustion chamber. The dimensions of the nozzle vary according to the engine power. In the straight-cut throat section, the diameter is D, and its straight length is L. Rogers [37] proposes as design criteria for straight-cut throat nozzles the length-to-diameter ratio $L/D \leq 0.4$ since the nozzle performance losses increase for higher values of $L/D > 0.4$. The loss mechanisms are divided into three categories: internal nozzle wall geometry losses, viscous drag losses, and chemical kinetic losses [1,37]. Of the diversity of rocket engines, as a reference, we mention the TU-223 Mace Booster solid fuel rocket engines of length $L_m = 3.27$ m and conical nozzle with L/D = 0.303; and the TE-M-388 Iroquios engine of length $L_m = 2.65$ m and conical nozzle with L/D = 0.952; both of which have been reported by Rogers [37].

Tolentino and Mírez [38], applying CFD, performed numerical studies on the effect of throat length on the flow development in conical nozzles with straight-cut throat, for $L/D = 1.5$. They reported that, in the throat section, the flow presents oblique shocks (shock train) in the estimated range from Mach number 0.65 to 1.74, the fluctuation being more intense at the beginning of the throat section and less intense at the end of the throat section. Also, numerical studies on the flow de–velopment in straight-cut throat conical nozzles for L/D ≈ 1 reported oblique shocks in the throat section, where the flow exhibits velocity fluctuations in the estimated range from Mach number 0.75 to 1.55 [39-41].

In contrast, for convergent-divergent conical nozzles that have a radius of curvature at the wall of the throat section, oblique shocks are not present, and the study of the radius of curvature has been addressed by Sauer [42], Cuffel et al. [43], and Back et al. [44].

Based on the aforementioned studies on the flow behavior in the presence of the shock train, the study of the flow in planar nozzles with straight-cut throats has been motivated. In this sense, the present investigation aims to analyze the behavior of compressible flow in planar nozzles with straight-cut throats and to determine the range of velocity and pressure fluctuations in the throat section. Section 2 presents the applied metho–dology. Section 3 analyses the results of the flow field simulations. Finally, section 4 presents the conclusions.

2.   METHODOLOGY

2.1 Planar nozzle

For the study of the compressible flow field in planar nozzles, applying CFD, the geometry of the off-design

planar nozzle of the Hunter paper [10], shown in Fig. 1, has been taken into consideration. The planar nozzle [10] is an experimental equipment belonging to the NASA Langley 16-Foot Transonic Tunnel Complex.
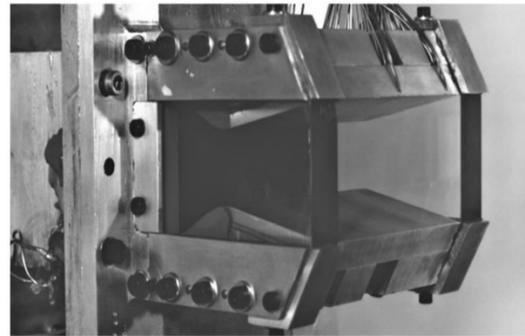
Figure 1. Experimental equipment: off-design planar nozzle [10].

Based on isentropic flow theory, the planar nozzle in the Hunter work [10] is designed for a flow adapted for NPR=8.78, Mach number 2.07 at the nozzle outlet, and an atmospheric pressure of 102.387 kPa (14.85 psi).

The schematic of the planar nozzle geometry [10] is shown in Fig. 2a. The main dimensions of the planar nozzle are the throat cross-sectional area $A_t = 2785.1557$ mm^2, the expansion ratio $A_e/A_t = 1.797$, where the exhaust area is A_e and the nozzle width 101.346 mm. The convergent has a half angle $\beta = 27.29°$, and the divergent has a half angle $\alpha = 11.01°$. The throat wall has a curvature of radius $R_t = 15.875$ mm (0.625 in). The air mass flow rate is supplied to the nozzle up to a capacity of 6.804 kg/s (15 lbm/sec), with a stagnation temperature control of 294.444 K (530 R) [10].
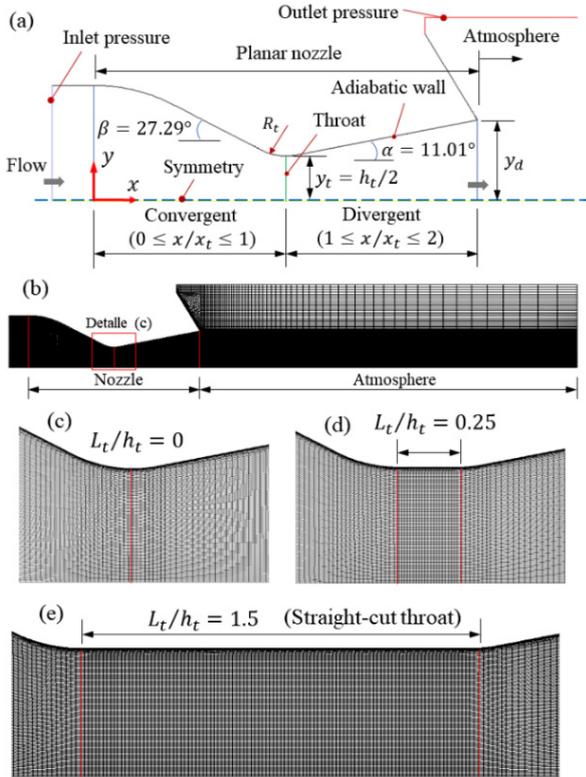
2.2 Computational domain, meshing, and boundary conditions

The geometry of the planar nozzle shown in Fig. 2a was modified in the throat section by the authors of the present investigation. A straight-cut throat was added between the convergent and divergent throat, and the length of the throat L_t/L_h, where L_t is the straight length of the throat and h_t is the height of the throat, was taken as a variable parameter. In the throat section, the mean height is $y_t = h_t/2$, and at the divergent outlet, the mean height is y_d. The convergent and divergent geometrical parameters were not changed, so their original design was maintained. The radius of curvature at the end of the convergent and at the beginning of the divergent is $R_t = 15.875$ mm (0.625 in) [10].

It was taken into consideration to simulate the flow adapted for NPR = 8.78, for 2D computational domains, and this is due to the symmetry it presents. Fig. 2 illus-trates the planar nozzle's schematic and the compu-tational domains' meshing.

The computational domain is illustrated in Fig. 2a, where the boundary conditions are applied. For the flow study, seven planar nozzle geometries were considered, with the first nozzle without throat length $L_t/L_h = 0$ (Fig. 2c) and the other six nozzles with throat length for increments of 0.25 up to $L_t/L_h = 1.5$. It should be noted that details for $L_t/L_h = 0.5$, $L_t/L_h = 0.75$, $L_t/L_h = 1$, and $L_t/L_h = 1.25$ are not included in Fig. 2. Table 1 presents

the convergent, throat length and divergent positions of the seven planar nozzles. It should be noted that the computational domain geometries of the seven planar nozzles were performed in the ANSYS-Geometry platform.

Figure 2. (a) Computational domainandboundary conditions for the geometry of a planar nozzle. (b) Meshed domain (mesh 3).Enlargement of details (c), (d), and (e)of the throat section.

The domains meshed in the ANSYS-Meshing platform, and the domains were discretized using ICEM-CFD interaction. Fig. 2b illustrates the meshed computational domain with 28930 elements (mesh 3), comprising the nozzle and a region of the atmosphere. Fig. 2c shows the detail for a meshed region of the throat section for $L_t/L_h = 0$, which corresponds to the wall curvature of the original planar nozzle design from research work by Hunter [10]. Fig. 2d shows the mesh region for throat length $L_t/L_h = 0$ and Fig. 2e for $L_t/L_h = 1.5$. The meshing in the wall regions has been refined due to the presence of shear stresses. It should be noted that the meshing details for other sections of the throat length are not presented, as the distribution of cells in the mesh is similar.

The parameters of the boundary conditions were set as follows. For the flow in the atmosphere: static pressure $p = 102.387$ kPa and static temperature $T = 294.444$ K. For the flow at the nozzle inlet: total pressure $p_0 = 898.9798$ kPa and total temperature $T_0 = 294.444$ K. The nozzle pressure ratio is expressed as NPR = $p_0/p = 8.78$.

The nozzle walls in the computational domain were considered adiabatic walls, so there is no heat transfer through the wall. The flow velocity is zero in the adiabatic wall due to the no-slip condition. In symmetry, in the y-axis direction, the velocity is zero. The

effect of gravity has not been taken into account throughout the 2D computational domain. It should be noted that the flow parameters are taken from the work of Hunter [10].

Table 1. Range of convergent section, throat length, and divergent.

L_t/h_t	Convergent (x/x_t)	Throatlength (x/x_t)	Divergent (x/x_t)
0.0	0 - 1	1	1 - 2
0.25	0 - 1	1 – 1.1189	1.1189 - 2.1189
0.50	0 - 1	1 – 1.2378	1.2378 - 2.2378
0.75	0 - 1	1 – 1.3567	1.3567 - 2.3567
1.0	0 - 1	1 – 1.4756	1.4756 - 2.4756
1.25	0 - 1	1 – 1.5945	1.5945 - 2.5945
1.5	0 - 1	1 – 1.7134	1.7134 - 2.7134

2.3 Mathematical fundamentals

The flow used is air, and it was considered as an ideal gas. The physical parameters of the air are as follows: the specific heat ratio being $k = 1.4$, the specific heat at constant pressure $C_p = 1006.43$ J/(kg·K), the thermal conductivity $k_t = 0.0242$ W/(m·K), and the constant of the gas $R = 287$ J/(kg·K) [45].

For compressible flow, the dominant parameter is the Mach number M, and is classified as: for incompressible flow $M < 0.3$; subsonic flow $0.3 \le M \le 0.8$; transonic flow $0.8 \le M \le 1.2$; supersonic flow $1.2 \le M \le 5$; hypersonic flow $M > 5$; sonic flow $M = 1$ [16].

The flow field was simulated in a steady state in the ANSYS Fluent R16.2 code [45], and the Reynolds-averaged Navier-Stokes (RANS) equations were used. The governing equations, such as the mass conservation equation (1), the momentum equation (2), the energy equation (3), and the ideal gas equation of state (4) [45], in compact form are expressed as:

$$\nabla \cdot (\rho u_i) = 0 \tag{1}$$

$$\nabla \cdot (\rho u_i u_j) = -\nabla p + \nabla \cdot (\overline{\overline{\tau}}) + \nabla \cdot (-\rho \overline{u'_j u'_j}) \tag{2}$$

$$\nabla \cdot (u_i (\rho E + p)) = \nabla \cdot (k_{eff} \nabla T + (\overline{\overline{\tau}}_{eff} \cdot u_i)) \tag{3}$$

$$p = \rho R T \tag{4}$$

The parameters of the above equations are as fol–lows: ρ is the density; u is the velocity; p is the pressure; T is the temperature, and R is the ideal gas constant. $\overline{\overline{\tau}}_{eff}$ is the stress tensor, and $-\rho \overline{u'_j u'_j}$ are the Reynolds stresses. E is the total energy; k_{eff} is the effective thermal conductivity, and $\overline{\overline{\tau}}_{eff}$ is the effective stress tensor.

The Sutherland equation [46] was used for viscosity as a temperature function. The Spalart-Allmaras turbu–lence model [47] was used to simulate turbulence.

2.4 Computational solution method

The ANSYS-Fluent R16.2 code [45], which applies the finite volume method (FVM) [26], was used for the flow field simulations. The following considerations

have been taken into account:density-based, time-steady, planar 2D. The Roe-FDS flow type was applied, as well as Least Squares Cell Based. The Second Order Upwind option was applied for the flow, kinetic energy turbulence, and specific dissipation. As a control para–meter in the iterations, it was taken into account for the mass flow rate, for the error in the range of 1×10^{-4} to 1×10^{-6}. The hybrid initialization method was applied.To obtain the solutions of the computational simulations, iterations were performed in the range of 24900 to 86900. The computer used for the computational simulations has the following characteristics: Dell CPU, model Optiplex 7010, i5 3470, four processors of3.2 GHz, and 8 GB of RAM.

2.5 Numerical convergence analysis

A sensitivity analysis was performed for three meshed domains for the original design planar nozzle ($L_t/h_t = 0$) for the evaluation of y^+ in the shear stress value (Fig. 3). Where mesh 1 has 28010 elements, mesh 2 has 28493 elements, and mesh 3 has 28930 elements.All three meshed domains were evaluated for the Spalart-Allmaras turbulence model [47] for NPR = 8.78. The magnitudes of y^+ were obtained, being smaller for mesh 3. The region of the highest magnitude of y^+occurs for the flow near the divergent outlet at the estimated position $x/x_t \approx 0.93$, where $y^+ < 103$.
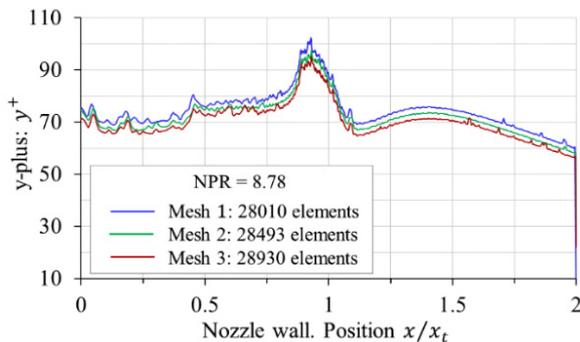
Figure 3. y^+ curves evaluated on the walls of the planar no–zzle. Range: convergent $0 \leq x/xt \leq 1$; divergent $1 \leq x/xt \leq 2$.

For mesh 3, at the nozzle outlet, the average value of Mach number 2.0046 for the viscous flow was obtained for the 2D simulation, which is slightly close to the value of Mach number 2.07 for the isentropic flow of the nozzle design, with an absolute error of 0.065. Therefore, the meshed domain for mesh 3 is acceptable for simulating the adapted flow field.

2.6 Validationof the Spalart-Allmaras turbulence model

The Spalart-Allmaras S-A turbulence model [47] was validated with the experimental pressure data reported by Hunter [10] for NPR = 3.413 (Fig. 4); also, the S-A [47] model was compared with SST$k - \omega$ of Menter [48], standard $k - \omega$ turbulence models of Wilcox [49] and RSM of Launder et al. [50].The S-A turbulence model curve presented the best fit for the critical region where the lowest pressure drop is present with respect to the experimental data [10]; for the position $x/x_t = 1.717$, a position error of 0.32% was obtained. While the

curves of the SST$k - \omega$ [48] and $k - \omega$ [49] turbulence models are shifted to the left and RSM [50] to the right, for which positional errors of more than 1.68% were obtained.

The Spalart-Allmaras turbulence model [47] is a one-equation model, and its trajectory shows that it res–ponds better to adverse pressure gradients and boundary layer separation than the other three turbulence models used.
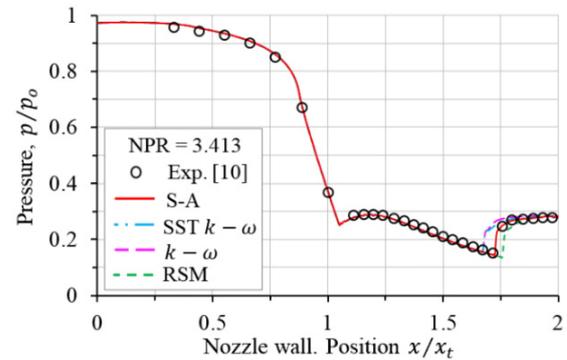
Figure 4. Comparison of curves from computational simulations and experimental pressure data [10]. Range: convergent 0 ≤ x/xt ≤ 1; divergent 1 ≤ x/xt ≤ 2

3. RESULT AND DISCUSSION

This section presents the flow field simulations for the planar nozzles with throat length: $L_t/h_t = 0$, $L_t/h_t = 0.25$, $L_t/h_t = 0.5$, $L_t/h_t = 0.75$, $L_t/h_t = 1$, $L_t/h_t = 1.25$ and $L_t/h_t = 1.5$. Table 1 presented above indicates the positions of the convergent ranges, the length of the throat, and the divergent range. In the flow field figures, red regions represent higher magnitude values, and blue regions represent lower magnitude values.

3.1 Flow field: Mach number

The Mach number flow field for each case of the planar nozzle with throat length from $L_t/h_t = 0$ to $L_t/h_t = 1.5$ are shown in Fig. 5. The internal shocks, which are oblique shock waves, are observed at the throat, at divergent, and at the nozzle outlet. The curve trajectories of the Mach number patterns evaluated at the nozzle symmetry for each throat length L_t/h_t are shown in Fig. 6.

For $L_t/h_t = 0$ (Fig. 5a), there is no throat length, with $L_t = 0$. In Fig. 6 for $L_t/h_t = 0$, the flow in the throat section is observed to accelerate undisturbed.

In the throat section, starting from $L_t/h_t = 0.25$ (Fig. 5b and Fig. 6) up to $L_t/h_t = 1.5$ (Fig. 5g and Fig. 6), it is observed that as the throat length L_t/h_t increases, the evolution of internal shocks increases, the flow accelerates and decelerates, and the fluctuation towards the throat outlet decreases for $L_t/h_t = 1.5$, thus having a shock train. On the other hand, the flow in the divergent is accelerated, and its behavior undergoes slight changes due to the effect of the throat length, which causes variations in the intensity of the pressure waves in the flow regime at the throat outlet. The flow behavior is evident for the Mach number patterns shown in Fig. 6. For $L_t/h_t = 0.25$ (Fig. 5b and Fig. 6), the throat length is in the interval $1 \leq x/x_t \leq 1.1189$, the flow at the throat exit reaches Mach 1.16, then continues to accelerate at the divergent up to the position $x/x_t = 1.1445$ and

reaches Mach 1.205, and then slows down at position $x/x_t = 1.1780$ and reaches Mach 1.023, and then continues its fluctuating trajectory to the nozzle exit. For $L_t/h_t = 0.5$ (Fig. 5c and Fig. 6), the throat length is in the interval $1 \leq x/x_t \leq 1.2378$ and spans the Mach number behavior pattern up to the $x/x_t = 1.1780$ position for $L_t/h_t = 0.25$ (Fig. 6). Thus, as the throat length increases up to $L_t/h_t = 1.5$ (Fig. 6), the sections of curve trajectories of shorter throat lengths overlap with those of longer lengths, and the fluctuations decrease towards the throat exit. Therefore, increasing the throat length reduces the flow velocity in that section. For $L_t/h_t = 1.5$ (Fig. 5g and Fig. 6), the flow velocity in the throat section is in the range of $1 \leq M \leq 1.2$ and exhibits four peaks of Mach number values. The first peak occurs at position $x/x_t = 1.445$ for Mach 1.205, the second peak at $x/x_t = 1.3297$ for Mach 1.123, the third peak at $x/x_t = 1.492$ for Mach 1.087, and the fourth peak at $x/x_t = 1.618$ for Mach 1.062. The peaks of the flow velocity occur in the regions of the intersections of the oblique shocks in the throat section, seen in Fig. 5, from $L_t/h_t = 0.5$ to $L_t/h_t = 1.5$. For $L_t/h_t = 0.25$, the peak is outside the throat, at the beginning of the divergent.

Fig. 7 shows the trajectories of the Mach number curves at the throat length exit for the range of $L_t/h_t = 0$ to $L_t/h_t = 1.5$, which are related to Fig. 6 and 5. It is observed that for $L_t/h_t = 0$, the flow in the central region is close to Mach 0.9, whereas, for the flow in the near-wall region within the range of $0.9 \leq y/y_t \leq 1$, an estimated peak of Mach 1.25 is presented.

As the throat length increases, the fluctuations decrease to a horizontal trend behavior for the range of $0 \leq y/y_t \leq 0.9$, where the flow approaches the sonic velocity, Mach 1. Slight increases in fluctuation occur for the range of $0.9 \leq y/y_t \leq 1$, where the flow reaches values below Mach 1.2. The best behavior of the horizontal trend curve occurs for $L_t/h_t = 1.5$.

The throat length slightly affects the flow at the nozzle outlet, as shown in Fig. 8. For the flow region adjacent to the wall in the range of $0.9 \leq y/y_d \leq 1$ (detail (a)), the curve $L_t/h_t = 1.5$ is the furthest away from $L_t/h_t = 0$. This behavior is also affected by the thermal boundary layer and the shear stress in the flow region adjacent to the diverging wall, as the flow friction at the wall varies with respect to the flow velocity.

Table 2 presents the average values obtained by numerical integration for the Mach number curves at the throat outlet (Fig. 7) and at the nozzle outlet (Fig. 8). The same table includes the percentage errors based on the Mach 1 isentropic flow for the throat section, and for the viscous flow velocity at the nozzle outlet of Mach 2.07 [10].

With respect to the flow at the throat outlet, the smallest Mach number error is 0.29% for $L_t/h_t = 0$, and the largest error is 8% for $L_t/h_t = 0.5$. For $L_t/h_t = 1.5$, the error decreases to 4.4%.

For the flow at the nozzle outlet, the average Mach number decreases progressively from Mach 2.0046 ($L_t/h_t = 0$) to Mach 1.9981 ($L_t/h_t = 1.5$), while the error increases in the range of 3.15% to 3.47%. Therefore, by decreasing the flow velocity at the nozzle outlet, the thrust force will also decrease as the throat length

increases. Consequently, throat length has a significant effect on the flow regime.
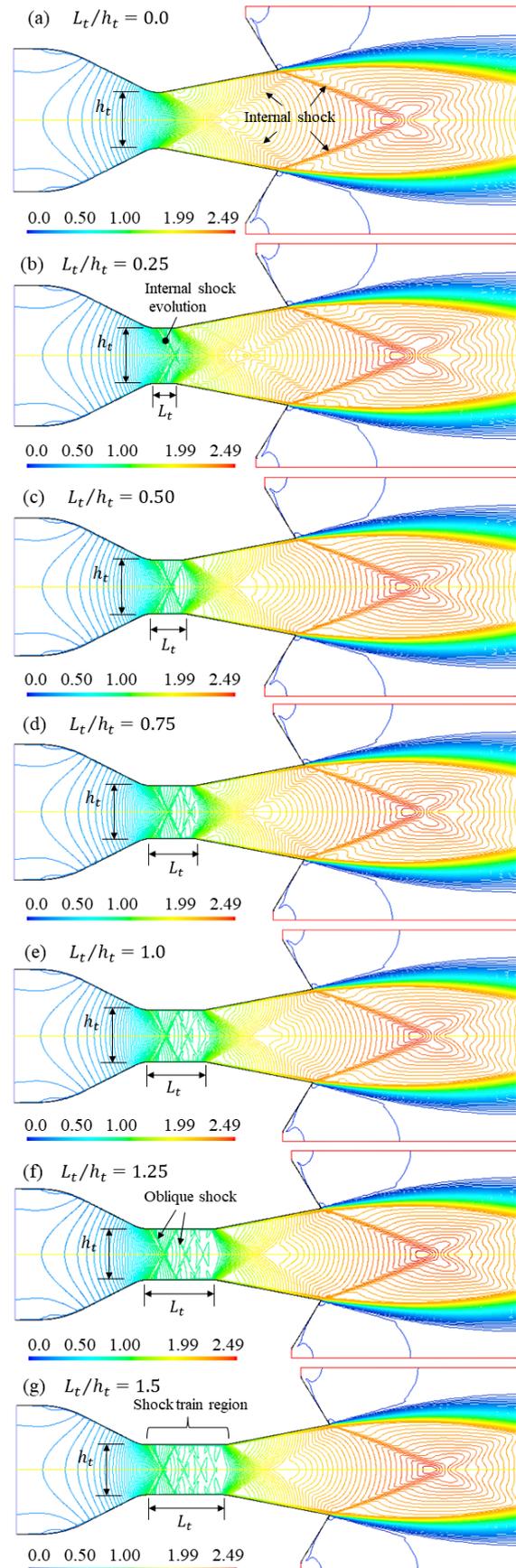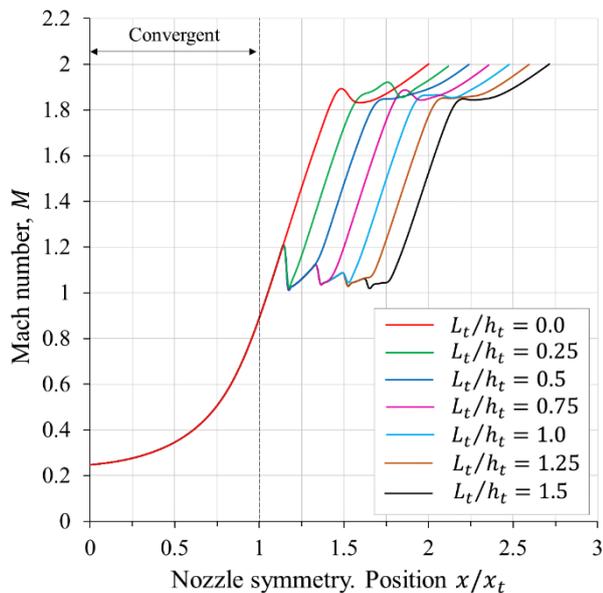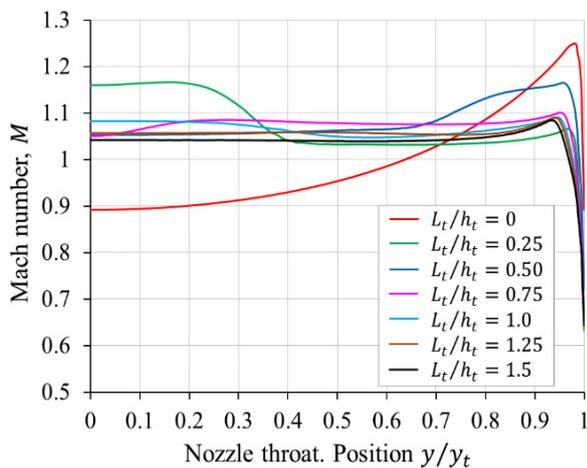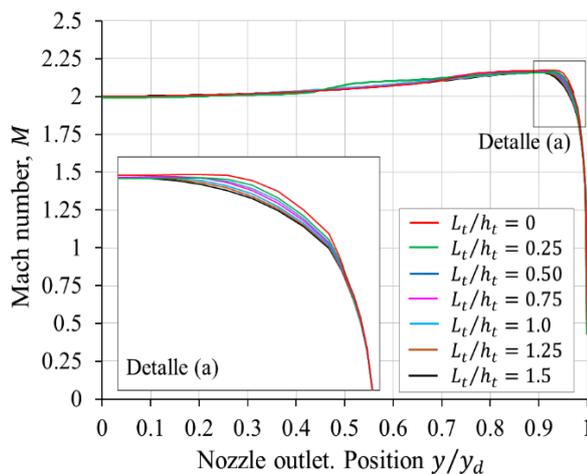

Figure 5. Flow field: Mach number contour lines. Evolution of internal shock formation in the throat section. Throat length ranges from $L_t/h_t = 0$ to $L_t/h_t = 1.5$. Flow for NPR=8.78.

Figure 6. Mach number patterns evaluated in symmetry. Throat length ranges from $L_t/h_t = 0$ to $L_t/h_t = 1.5$.

Figure 7. Mach number patterns are evaluated in the y-axis direction at the throat exit.


Figure 8. Mach number patterns are evaluated in the y-axis direction at the nozzle exit.

Fig. 9 is part of Fig. 5, which illustrates the velocity and discharge distribution of the supersonic jet in the region of the atmosphere for the nozzle with $L_t/h_t = 0$ (Fig. 9a) and $L_t/h_t = 1.5$ (Fig. 9b).

Table 2. Average values of the Mach number and percen–tage errors were evaluated at the outlet of the throat and nozzle.

Throat: L_t/h_t	Throatoutlet		Nozzleoutlet	
	Mach number	Error (%)	Mach number	Error (%)
0.0	1.0029	0.29	2.0046	3.15
0.25	1.0789	7.89	2.0043	3.17
0.50	1.0800	8.00	2.0025	3.25
0.75	1.0751	7.51	2.0015	3.30
1.0	1.0650	6.50	2.0004	3.36
1.25	1.0561	5.61	1.9992	3.41
1.5	1.0440	4.40	1.9981	3.47
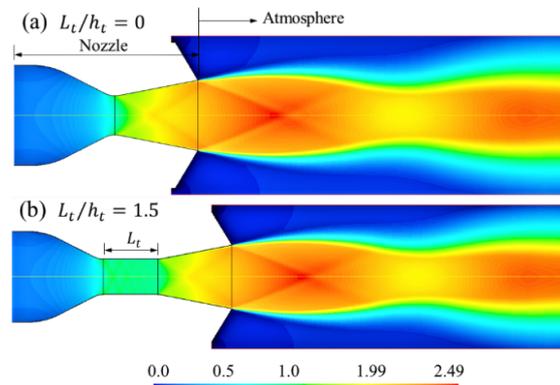
Figure 9. Mach number flow field: (a) Nozzle with $L_t/h_t = 0$ and (b) Nozzlewith $L_t/h_t = 1.5$.
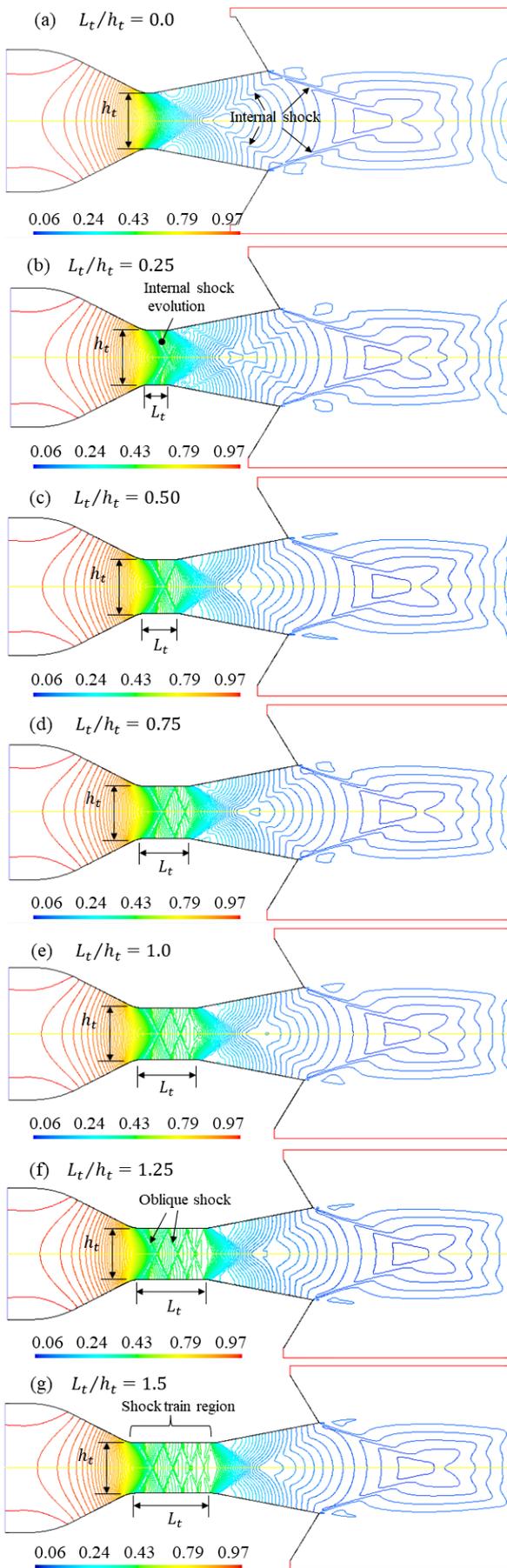
3.2 Flow field: Static pressure

The flow field for the static pressure is shown in Fig. 10, for $L_t/h_t = 0$ to $L_t/h_t = 1.5$, where it is observed how the flow pressure is distributed in the convergent, throat, and divergent. These results are related to the flow field for the Mach number presented in Fig. 5.

The evolution of the oblique shock formation in the throat section starts from $L_t/h_t = 0.25$, and for $L_t/h_t = 1.5$, the formation of oblique shock waves forming the shock train region is defined.
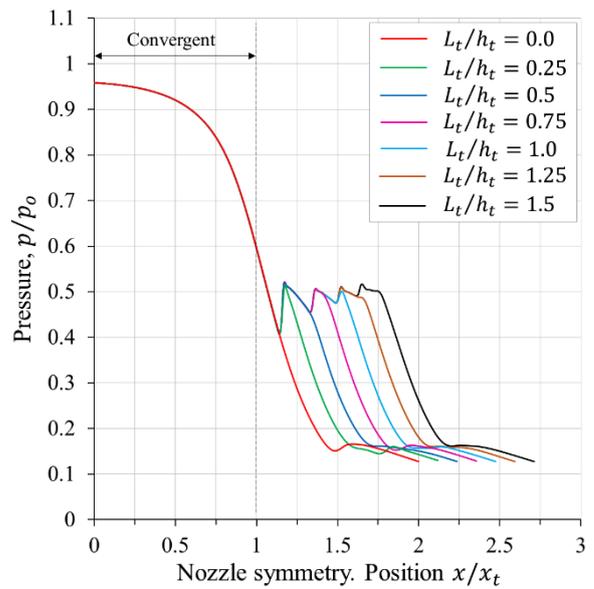
The static pressure patterns evaluated at the sym–metry and at the nozzle wall are shown in Fig. 11 and Fig. 12, which are related to Fig. 10. In the throat section, for $L_t/h_t = 0$, the flow pressure decreases wit–hout interruption. In contrast, from $L_t/h_t = 0.25$, the flow pre–ssure fluctuates, and the fluctuation at the throat outlet decreases as the throat length increases. For $L_t/h_t = 1.5$, the pressure difference is in the range of $0.4 \leq p/p_0 \leq 0.52$.

The pressure patterns evaluated at the nozzle wall, which are the lateral pressure loads, are shown in Fig. 12. In the throat section, for $L_t/h_t = 1.5$, the pressure difference is in the range of $0.37 \leq p/p_0 \leq 0.52$. The fluctuating pressure gradients affect the development of the flow regime, where the flow velocity fluctuates towards the wall until it stops upon contact with the nozzle wall. In the throat section, the oblique shocks are more intense for the region of the shock train, and at the end of the throat length, the fluctuations decrease.

Fig. 13 is a part of Fig. 10, which illustrates the static pressure distribution in the nozzle and in the atmospheric region, for the nozzle with $L_t/h_t = 0$ (Fig. 13a) and $L_t/h_t = 1.5$ (Fig. 13b).

Figure 10. Flow field: Static pressure contour lines. Evolution of internal shock formation in the throat section. Throat length ranges from $L_t/h_t = 0$ to $L_t/h_t = 1.5$. Flow for NPR=8.78.

Figure 11. Static pressure patterns evaluated in symmetry. Throat length ranges from $L_t/h_t = 0$ to $L_t/h_t = 1.5$.
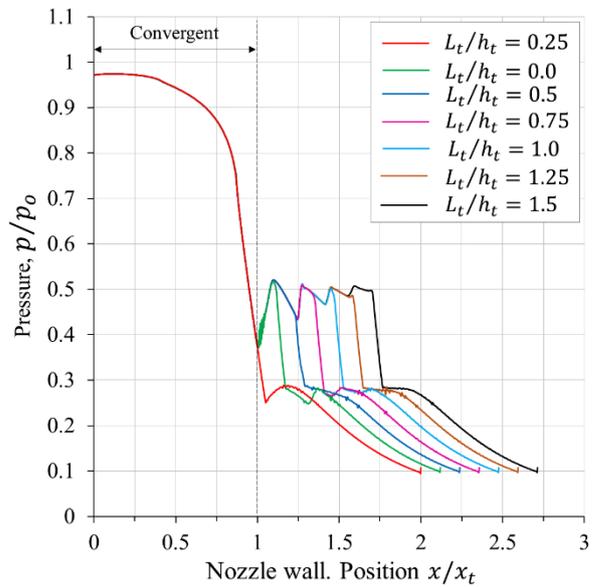
**Figure 12. Static pressure patterns were evaluated at the wall. Throat length ranges from $L_t/h_t = 0$ to $L_t/h_t = 1.5$.**
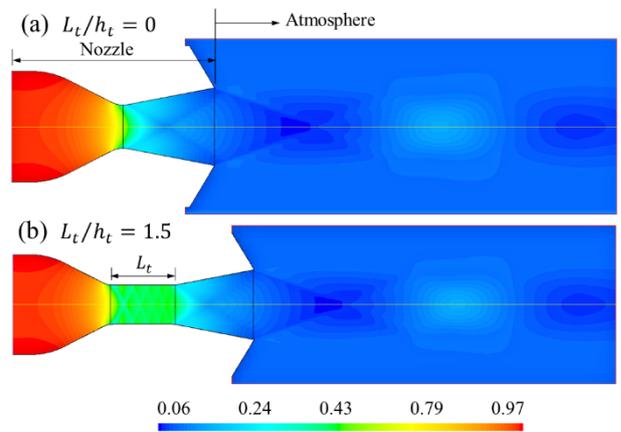
Figure 13. Static pressure flow field: (a) Nozzle with $L_t/h_t = 0$ and (b) Nozzle with $L_t/h_t = 1.5$.

The static pressure from the computational simula–tions, evaluated at the divergent walls of the planar nozzles, for throat lengths $L_t/h_t = 0$ to $L_t/h_t = 1.5$, are

compared with the experimental pressure data from the Hunter paper [10], for NPR=8.78, as shown in Fig. 14. Where, the divergent positions, for $L_t/h_t = 0.25$, $L_t/h_t = 0.5$, $L_t/h_t = 0.75$, $L_t/h_t = 1$, $L_t/h_t = 1.25$, and $L_t/h_t = 1.5$, have been taken to the relative position with respect to the nozzle with $L_t/h_t = 0$ since all nozzles have the same divergent length.
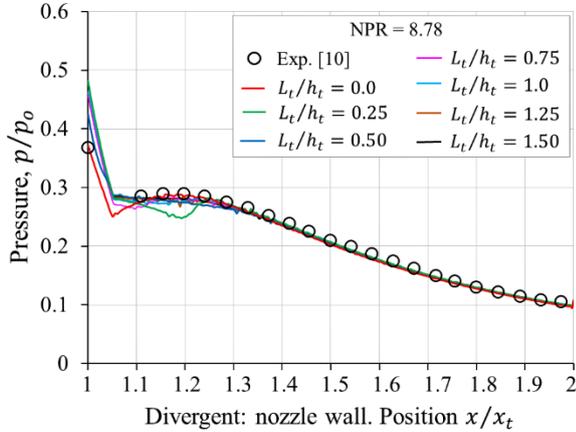
Figure 14. Comparison of simulation curves with experi– mental pressure data [10].

It is observed in the above figure (Fig. 14) that the fit of the curve trajectory for $L_t/h_t = 0$ with the expe– rimental pressure data [10]. While the curves for $L_t/h_t = 0.25$, $L_t/h_t = 0.5$, $L_t/h_t = 0.75$, $L_t/h_t = 1$, $L_t/h_t = 1.25$, and $L_t/h_t = 1.5$ present different pressure magnitudes at the divergent inlet. In the range of $1 \leq x/x_t \leq 1.3$, the flow fluctuates due to the effect of throat length. For the range of $1.3 \leq x/x_t \leq 2$, the curves overlap along with the curve $L_t/h_t = 0$, and the effect of throat length is slightly smaller with respect to the mentioned range of $1 \leq x/x_t \leq 1.3$.

3.3 Flow field: Density

For better visualization of the shock train in the throat section, the images are illustrated in greyscale for the density variations of the flow regime.

The flow density distribution at nozzle divergent without throat length ($L_t/h_t = 0$) for NPR=8.95 is shown in Fig. 15a. The image was captured with the Schlieren technique and corresponds to the experimental work of Hunter [10]. The density simulation obtained in the present work is shown in Fig. 15b.

The intersection of the oblique shock at the divergent occurs in the position range $1.4 \leq x/x_t \leq 1.6$, and the velocity fluctuation for $L_t/h_t = 0$ is shown in Fig. 6. It is observed that the distributions of the oblique shocks from the computational simulation in Fig. 15b and Fig. 9a are approximately similar to the image of the experiment shown in Fig. 15a.

The flow density distribution in the throat section for $L_t/h_t = 1.5$ and NPR=8.78 is shown in Fig. 16. The formation of oblique shocks is observed, where the highest intensity is in the left end region, and the lowest intensity is in the right end region. The flow regime in the throat section for $L_t/h_t = 1.5$, mentioned above: the patterns of the velocity fluctuations with respect to the

Mach number are shown in Fig. 6 and of the static pressures in Fig. 11 and Fig. 12.
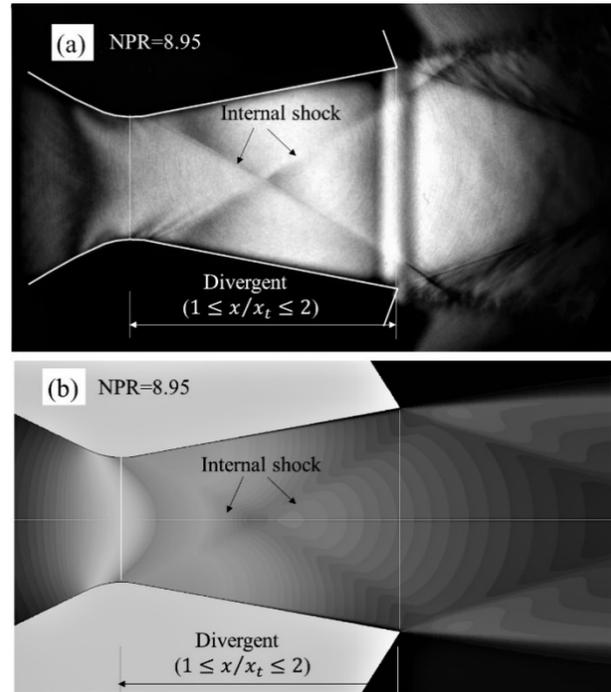
Figure 15. (a) Image captured with the Schlieren technique by Hunter [10]. (b) Simulation of the flow density.
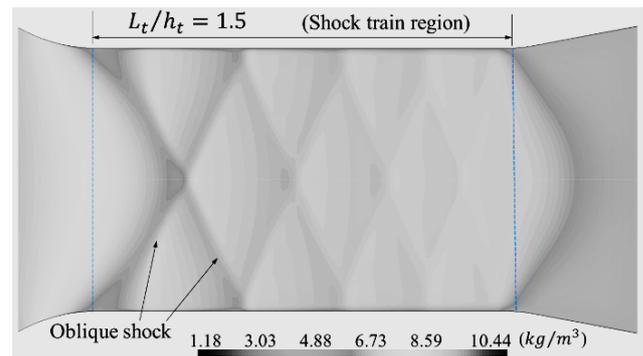
Figure 16. Flow density in the throat section. Distribution of oblique shocks forming the shock train region. Flow for NPR=8.78.

At the throat length of the planar nozzle, where the shock train region occurs, the flow velocity fluctuations are in the range of $1 \leq M \leq 1.2$, and whose magnitude range is smaller with respect to the throat length conical nozzle geometries reported in [38-41], which are in the estimated range of Mach number 0.65 to 1.74. There– fore, in the throat section, the geometries of the inner walls in the cross and longitudinal sections affect the propagation of the pressure waves in their development, and the interaction of the turbulent boundary layer with the oblique shock waves is affected in its structure by the pressure gradients that are distributed along the throat section.

It should be noted that the results obtained from the numerical simulations of the Mach number, pressure, and density flow field in the present investigation are approximations with certain margins of errors, where the most common types of numerical errors are the following: modeling errors, discretization errors, itera– tion errors, and programming and user errors [26].

For this reason, the pressure simulations on the divergent wall (Fig. 14) have been compared with the experimental data of the Hunter work [10]. However, further research must perform extension experiments for the planar nozzle studied by Hunter [10], incorporating a straight-cut throat to record with the Schlieren technique the region of the shock train in the throat section and the flow region in the divergent one and whose experimental results serve as a comparative standard for the computational simulations.

4. CONCLUSION

Computational simulations of the flow field in planar nozzles with straight-cut throats have made it possible to determine the effect of throat length on flow deve–lopment.

As the throat length increases from $L_t/h_t = 0.25$ to $L_t/h_t = 1.5$, internal shocks originate, and the shocks form a train of shocks. In symmetry, for $L_t/h_t = 1.5$, the fluctuation is strongest at the beginning of the throat and weakest at the end of the throat, where the flow accelerates and decelerates and is at transonic velocity in the Mach number range of $1 \leq M \leq 1.2$. Increasing the throat length slows down the flow velocity in the throat section. For the Mach number at the nozzle outlet, for $L_t/h_t = 1.5$, the largest error of 3.47% was obtained.

With respect to the static pressure in the throat section, for $L_t/h_t = 1.5$, the flow fluctuates in the range of $0.37 \leq p/p_0 \leq 0.52$.

Extended studies for nozzles with straight-cut throats in the range of $0 \leq L_t/h_t \leq 0.25$ are considered relevant in order to determine the magnitude of the flow fluctuation inside and at the throat outlet. Also, experimental studies of the flow for $0 \leq L_t/h_t \leq 1.5$, and higher values of $L_t/h_t > 1.5$, modifying the throat section of the experimental nozzle studied by Hunter [10], in order to compare the approximate numerical results obtained in the present work.

REFERENCES

[1] Sutton, G.P. and Biblarz, O.: *Rocket propulsion elements,* John Wiley and Sons, New York, 2016.

[2] Scarlatella, G., Tajmar, M., and Bach, C.: Advanced nozzle concepts in retro-propulsion applications for reusable launch vehicle recovery: a case study, in:*72nd International Astronautical Congress (IAC),* Dubai, United Arab Emirates, 25-29 October, 2021.

[3] Hagemann, G., Preusss, A., Grauer, F., Krestschmer, J., Frey, M., Ryden, R., Stark, R. and Zerjeski, D.: Technology investigation for high area ratio nozzle concepts, in: *39th AIAA/ASME/SAE/ASEE Joint Propulsion conference and Exhibit,* 20-23 July 2003, Hunstville, Alabama.

[4] Stark, R. and Hagemann, G.: Current status of numerical flow prediction for separated nozzle flows, in: *2 European Conference for Aerospace Sciences (Eucass),* 2007.

[5] Östlund, J., Muhammed-Klingmann, B.: Supersonic flow separation with application to rocket engine nozzles, ASME, Applied Mechanics Reviews, Vol. 58, No. 3, pp. 143–177, 2005.

[6] Nagamatsu, H.T. and Scavallo, P.G.: An experimental and theoretical study of a D.C. arc in a 30° conical nozzle flow, *18th Aerospace Sciences meeting,* January 14-16, 1980,Pasadena, California.

[7] Back, L.H., Massier, P.F. and Cuffel, R.F.: Flow phenomena and convective heat transfer in a conical supersonic nozzle, *Journal spacecraft,* Vol. 4, No. 8, pp. 1040-1047, 1967.

[8] Jia, R. Jiang, Z. and Zhang, W.: Numerical analysis of flow separation and side loads of a conical nozzle during staging, *Journal Aerospace Engineering,* Vol. 230, No. 5, pp. 845-855, 2016.

[9] Malina, F.J.: Characteristics of the rocket motor based on the theory of perfect gases, *J. Frankling Inst.,* Vol. 230, No. 4, pp. 433-454, 1940.

[10] Hunter, C.A.:Experimental investigation of sepa–rated nozzle flows, *Journal of Propulsion and Po–wer,* Vol. 20, no. 3, pp. 527-532, May-June, 2004.

[11] Arora, R., Vaidyanathan, R.: Experimental inves–tigation of flow through planar double divergent nozzles, *Acta Astronautica,* Vol. 112, pp. 200-216, 2015.

[12] Živković, S., Milinović, M., Adamec, N.: Experi–mental and numerical research of a supersonic planar thrust vectoring nozzle via mechanical tabs, *FME Transactions*, Vol. 42, No. 3, pp. 205-211, 2014.

[13] Li, Y. He, Ch., Li, J., Miao, L., Gao, R. and Liang, J.: Experimental investigation of flow separation in a planar convergent-divergent nozzle, *Journal of Physics: Conference Series, 1300, 012088,* 2019.

[14] Hagemann, G., Immich, H., Nguyen, T. and Dumnov, G.E.: Advanced rocket nozzles, *Journal of Propulsion and Power,* Vol. 14, No. 5, pp.620-634, 1998.

[15] Rao, G.V.R.: Exhaust nozzle contour for optimum thrust, *Journal of Jet Propulsion,* Vol. 28, No. 6, pp. 377-382, 1958.

[16] Anderson, J.D: *Fundamentalsof aerodynamics*, New York, McGraw-Hill Education, 2017.

[17] Ferrari, A.: Exact solutions for quasi-one-dimensional compressible viscous flows in conical nozzles, *Journal of Fluid Mechanics*, vol. 915, pp. 1-21, 2021.

[18] Majdalani, J. and Maicke, B.: Explicit inversion of stodola´s area-Mach number equation, *Journal of Heat Transfer*, Vol. 133, No. 7, pp. 071702 1-7, 2011.

[19] Tolentino, S.L.: Comparative analysis of 2D simulations and isentropic equations for compressible flow in experimental nozzles, *INCAS BULLETIN*, Vol. 15, No. 3, pp. 111-115, 2023.

[20] Tolentino, S.L.: Empirical equation of the Mach number as a function of the stagnation pressure ratio for a quasi-one-dimensional compressible flow, *FME Transactions*, Vol. 51, No. 2, pp. 149-160, 2023.

[21] Schlichting, h. and Gersten, k.: *Boundary-layer theory*, Berlin Heidelberg, Germany, Springer Verlag, 9th ed., 2017.

[22] Hadjadj, A., Ben-Nasr, O. Shadloo, M.S. and Chaudhuri, A.: Effect of wall temperature in supersonic turbulent boundary layers: A numerical study, *International Journal of Heat and Mass Transfer,* Vol. 81, pp. 426-438, 2015.

[23] Zmijanović, V., Rašuo, B. and Chpoun, A.: Flow separation modes and side phenomena in an overexpanded nozzle, *FME Transactions*, Vol. 40, No. 3, pp. 111-118, 2012.

[24] Hirai, R. and Kawai, S.: Wall pressure fluctuations in wall heated and cooled shock wave and turbulent boundary layer interactions, *International Journal of heat and fluid flow,* Vol. 103, October, 2023.

[25] Krehl, P. and Engemann, S.: August Toepler - the first who visualized shock waves, *ShockWaves*, Vol. 5, No. 1, pp. 1–18, 1995.

[26] Ferziger, J.H., Perić, M. and Street, R.L.: *Computational Methods for Fluid Dynamics*, Springer, 2020.

[27] Zebiri, B. Piquet, A., Hadjadj, A. and Verma, S.B.: Shock-induced flow separation in an overexpanded supersonic planar nozzle, *AIAA Journal,* Vol. 58, No. 5, pp. 2122-2131, 2020.

[28] Tolentino, S.L.: Evaluation of turbulence models for the air flow in a planar nozzle, *Ingenius,* No. 22, pp. 25-37, 2019.

[29] Tolentino, S.L., Mírez, J. and González, O.: Numerical analysis of the flow field in a planar nozzle for different divergent angles, *Journal of Mechanical Engineering and Sciences,* Vol. 16, No. 4, pp. 9241-9252, 2022.

[30] Verma, S.B. and Manisankar, C.: Origin of flow asymmetry in planar nozzles with separation, *Shock Waves,* Vol. 24, No. 2, pp. 191-209, 2014.

[31] Kamali, R., Mousavi, S.M. and Binesh, A.R.: Three dimensional CFD investigation of shock train structure in a supersonic nozzle, *Acta Astronautica*, Vol. 116, pp. 56-67, 2015.

[32] Giglmaier, M., Quaatz, J.F. and Gawehn, T.: Numerical and experimental investigations of pseudo-shock systems in a planar nozzle: impact of bypass mass flow due to narrow gaps, *Shock Waves,* Vol. 24, No. 2, pp. 139-156, 2014.

[33] Vignesh, P.S., Kim, T.H. and Kim, H.D.: Numerical study on shock train characteristic in divergent channels, *Journal of Applied Fluid Mechanics,* Vol. 13, No. 4, pp. 1081-1092, 2020.

[34] Matsuo, K., Miyazato, Y. and Kim, H.D.: Shock train and psedo-shock phenomena in internal gas flows, *Progress in Aerospace Sciences,* Vol. 35, No. 1, pp. 33-100, 1999.

[35] Wang, C., Cheng, C., Cheng, K. and Xue, L.: Unsteady behavior of oblique shock train and boundary layer interactions, *Aerospace Science and Technology,* Vol. 79, pp. 212-222, 2018.

[36] Xue, L., Cheng, C., Wang, C., Zhang, L. Li, K. and Cheng, K.: Oblique shock train motion based on schlieren image processing, *Chinese Journal of Aeronautics,* Vol. 36, No. 3, pp. 30-41, 2023.

[37] Rogers, C.E.: The solid rocket motor-Part 4. Departures from ideal performance for conical nozzles and bell nozzles, straight-cut throats and rounded throats, *Tech series, High Power Rocketry magazine*, Orem, 2004.

[38] Tolentino, S.L. and Mírez, J.: Throat length effect on the flow patterns in off-design conical nozzles, *FME Transactions,* Vol. 50, No. 2, pp. 271-282, 2022.

[39] Tolentino, S.L., Parco, M.A., Caraballo, S., Lacruz, L., Marcano, V., Ferreira, J. and Mírez, J.: Numerical analysis of the flow behavior in the throat section of an experimental conical nozzle, *Journal Enfoque UTE*, Vol. 12, No. 1, pp. 12–28, 2021, (in Spanish).

[40] Tolentino, S.L. and González, O.: Numerical analysis of the over-expanded flow in the experimental conical nozzle ULA-1B out of design, *Lámpsakos*, No 25, pp. 1-13, 2021, (inSpanish).

[41] Tolentino, S.L. and Mírez, J.: Numerical análisis of over-expanded flow in the experimental ULA-2 conical nozzle out of design, *Lámpsakos*, No 24, pp. 33-47, 2020, (in Spanish).

[42] Sauer, A.: General characteristics of the flow through nozzles at near critical speeds, NACATM-1147, 1947.

[43] Cuffel, R.F. Back, L.H. and Massier, P.F.: Transonic flow field in a supersonic nozzle with small throat radius of curvature,*AIAA Journal*,Vol.7, No. 7, pp. 1364–1366, 1969.

[44] Back, and R.F. Cuffel, R.F.: Flow coefficients for supersonic nozzles with comparatively small radius of curvature throats, *AAIA Journal*, Vol. 8,No. 2, pp.196-198, 1970.

[45] ANSYS, Ansys Fluent, Theory guide.

[46] Sutherland, W.: The viscosity of gases and molecular force, *Philosophical Magazine series 5*, Vol. 36, No. 223, pp. 507–531, 1893,

[47] Spalart, P.R. and Allmaras, S.R.: A one-equation turbulence model for aerodynamic flows", *30th Aerospace Sciences Meeting and Exhibit, 06 January 1992 – 09*, Reno, NV, U.S.A, 1992, pp. 1-22.

[48] Menter, F.: Two equation eddy-viscosity turbulence models for engineering applications, *AIAA Journal*, Vol. 32, pp. 1598-1605, 1994.

[49] Wilcox, D.C.: Reassessment of the scale determining equation for advanced turbulence models, *AIAA Journal*, Vol. 26, No. 11, pp. 1299–1310, 1988.

[50] Launder, B.E., Reece, G.J. and Rodi, W.: Progress in the development of a Reynolds-stress turbulence closure, *Journal of Fluid Mechanics,* Vol. 68, No. 3, pp. 537-566, 1975.

NOMENCLATURE

A_t	Nozzle throat area
A_e	Nozzle outlet area
C_p	Specific heat at constant pressure
h_t	Throat height
K	Specific heat ratio
k_t	Thermal conductivity
L_m	Rocket motor length
L_t	Throat length
M	Mach number
p	Static pressure
p_0	Total pressure
R	Gas constant
Rt	Throat radius of curvature
T	Static temperature
T_0	Total temperature
x	x-axis in the Cartesian plane
x_t	Convergent and divergent lengths
y	y-axis in the Cartesian plane
y_d	Mean divergent height
yt	Mean throat height
y^+	y-plus, in the shear stress value
α	Half angle of the divergent
β	Half angle of the convergent
ρ	Density
L/D	Throat length/diameter ratio
L_t/h_t	Throat length/height ratio
2D	Two dimensions
CFD	Computational Fluid Dynamics
FVM	Finite volume method
NPR	Nozzle pressure ratio

НУМЕРИЧКА АНАЛИЗА ЕВОЛУЦИЈЕ УДАРНОГ ВОЗА У ПЛАНАРНИМ МЛАЗНИЦАМА СА ДУЖИНОМ ГРЛА

С.Л. Толентино, Х. Мирес, С.А. Карабаљо

У овом истраживању, анализирано је понашање компресибилног струјања у равним млазницама са дужином грла да би се одредио опсег брзине протока и флуктуације притиска у пресеку грла. Поље протока је симулирано у 2Д рачунарским доменима са АНСИС-Флуент Р16.2 кодом. РАНС модел је примењен за стационарни проток. Кориш–ћене главне једначине су очување масе, импулса, енергије и једначина стања идеалног гаса. За вискозитет као функцију температуре коришћена је Садерлендова једначина. За моделирање турбу–ленције струјања коришћен је Спаларт-Аллмарасов модел турбуленције, који је потврђен експеримен–талним подацима о притиску. У делу грла, за централни део тока, како се дужина грла повећава, проток флуктуира и успорава. Настају коси ударни таласи и формира се област ударног влака. Брзина струјања је транссонична и налази се у опсегу Маховог броја од 1 до 1,2, а статички притисак је у опсегу од 0,37 до 0,52. Због тога, као резултат флуктуација протока, дужина грла има значајан утицај на развој протока.